Development 138, 1663-1674 (2011) doi:10.1242/dev.060897


# Extensive scar formation and regression during heart regeneration after cryoinjury in zebrafish

**Juan Manuel González-Rosa, Víctor Martín, Marina Peralta, Miguel Torres and Nadia Mercader***

## SUMMARY

The zebrafish heart has the capacity to regenerate after ventricular resection. Although this regeneration model has proved useful for the elucidation of certain regeneration mechanisms, it is based on the removal of heart tissue rather than its damage. Here, we characterize the cellular response and regenerative capacity of the zebrafish heart after cryoinjury, an alternative procedure that more closely models the pathophysiological process undergone by the human heart after myocardial infarction (MI). Localized damage was induced in 25% of the ventricle by cryocauterization (CC). During the first 24 hours post-injury, CC leads to cardiomyocyte death within the injured area and the near coronary vasculature. Cell death is followed by a rapid proliferative response in endocardium, epicardium and myocardium. During the first 3 weeks post-injury cell debris was cleared and the injured area replaced by a massive scar. The fibrotic tissue was subsequently degraded and replaced by cardiac tissue. Although animals survived CC, their hearts showed nonhomogeneous ventricular contraction and had a thickened ventricular wall, suggesting that regeneration is associated with processes resembling mammalian ventricular remodeling after acute MI. Our results provide the first evidence that, like mammalian hearts, teleost hearts undergo massive fibrosis after cardiac damage. Unlike mammals, however, the fish heart can progressively eliminate the scar and regenerate the lost myocardium, indicating that scar formation is compatible with myocardial regeneration and the existence of endogenous mechanisms of scar regression. This finding suggests that CC-induced damage in zebrafish could provide a valuable model for the study of the mechanisms of scar removal post-MI.

**KEY WORDS: Zebrafish, Cryoinjury, Fibrosis, Scar regression, Epicardium, Heart regeneration**

## INTRODUCTION

Myocardial infarction (MI) is the most common cause of cardiac injury in humans and results in acute loss of large numbers of myocardial cells. Sudden induction of ischemia in MI triggers the death of cardiomyocytes throughout the affected region (Jennings et al., 1990). The necrotic muscle elicits an inflammatory cascade leading to leukocyte infiltration and the clearing of dead cells and matrix debris from the infarct zone. This results in healing and replacement of the damaged tissue with scar tissue. In the early post-infarction period, this scar provides mechanical support to the infarcted heart that is vital to preventing myocardial wall rupture. However, scarring progressively leads to profound changes in ventricular architecture and geometry, referred to as 'ventricular remodeling', which can ultimately lead to cardiac failure. For many years, the postnatal mammalian heart was considered a postmitotic organ with no self-renewal capacity, in which growth is achieved mainly by hypertrophy. Recent findings have challenged this view. It has become clear that, albeit to a limited extent, cardiomyocytes proliferate in the postnatal heart in humans and mice (Bergmann et al., 2009; Hsieh et al., 2007; Kajstura et al., 2010; Urbanek et al., 2010) and that cardiac proliferation can be stimulated by exogenous factors in culture (Bersell et al., 2009; Ieda et al., 2009).

In contrast to mammals, other vertebrates such as teleosts have a marked capacity to regenerate cardiac tissue after injury. Thus, characterization of the mechanisms underlying heart regeneration in teleosts might offer a way to identify novel strategies to overcome the limited regenerative response in mammals. The current model of heart regeneration in zebrafish is based on the resection of around 20% of the ventricular apex. Complete regrowth of the amputated region, including the coronary vasculature, myocardium and endocardial tissues is achieved at 60 days post-amputation (Poss et al., 2002; Raya et al., 2003), resulting in a functional heart (Kikuchi et al., 2010). The correlation between ventricular resection in zebrafish and mammalian myocardial infarction is, however, limited: ventricular resection does not involve ischemia-induced cell death and no cell debris needs to be removed prior to its replacement by de novo formed tissue. In addition, although scar formation has been reported during the post-resection healing process, it is composed mainly of fibrin fibers with only minor collagen depositions (Poss et al., 2002), and thus does not resemble post-MI scar formation in mammals.

The role of the epicardium during myocardial regeneration has attracted growing interest within the scientific community in recent years (Limana et al., 2010; Vieira and Riley, 2010). During development, signals derived from the epicardium stimulate growth of the underlying myocardium (Carmona et al., 2010; Lie-Venema et al., 2007). In addition, epicardial derived cells (EPDCs) delaminate from the embryonic epicardium through a process of epithelial-mesenchymal transition (EMT) to give rise to cell types such as coronary smooth muscle cells and fibroblasts. Little is known about the role of the epicardium in the adult heart, although in the zebrafish a role during cardiac homeotasis has been suggested (Wills et al., 2008). The epicardium has also been proposed to play a role during heart regeneration in zebrafish (Lepilina et al., 2006), since one of the first responses to ventricular damage is the re-expression of epicardial marker genes that are

Department of Cardiovascular Development and Repair, Centro Nacional de Investigaciones Cardiovasculares CNIC, Calle Melchor Fernández Almagro 3, Madrid 28029, Spain.

*Author for correspondence (nmercader@cnic.es)

**Accepted 5 January 2011**

usually expressed only during development. Activation of the epicardial marker genes *Tbx18* and the Wilms tumor protein encoding gene *Wt1* also takes place after coronary artery ligation in the mouse (Limana et al., 2009; Wagner et al., 2002), suggesting that tissue damage in adult animals reactivates the developmental gene regulatory network.

This study describes the use of cryocauterization as an alternative method for inducing cardiac injury in zebrafish and characterizes the damage caused and the proliferative and repair responses induced. We also present the use of the Tg(*wt1b:GFP*) line as a reporter line for monitoring the epicardial response in vivo during cardiac regeneration in the zebrafish and describe an increase in the epicardial layer upon cryoinjury. We found that, in contrast to the resection model, heart cryoinjury induced massive cell death and fibrotic scar formation, resembling the consequences of MI in mammals. Unlike mammals, however, the zebrafish is able to remove massive fibrotic heart lesions and to regenerate the lost tissue.

## MATERIALS AND METHODS

### Zebrafish husbandry

All experiments were conducted with adult zebrafish between 6 and 18 months of age, raised at a density of 3 fish/l. Animals were housed and experiments performed in accordance with Spanish bioethical regulations for the use of laboratory animals. Fish lines used were the wild-type WIK strain (ZIRC, Eugene, OR, USA), Tg(*fli1a:GFP*)*y1* (Lawson and Weinstein, 2002), Tg(*cmlc2:GFP*) (generated by A. Raya, IBEC, Barcelona, Spain) and Tg(*wt1b*:GFP) (line 1) (Perner et al., 2007).

### Cryocauterization

Animals were anesthetized by immersion into 0.04% tricaine (Sigma, St Louis, MO, USA) and immobilized by squeezing them ventral upwards into a foam holder mounted on a Petri dish. A small incision was made through the body wall and the pericardium using forceps and microdissection scissors, tearing the tissue rather than making a clean cut in order to facilitate healing. Once the pericardial sac was opened, the heart ventricle was exposed by gently squeezing the abdomen. A 0.3 mm diameter copper filament (Goodfellow, UK) linked to a polyamide tube (Parker Hanninfin, Cleveland, OH, USA) was cooled in liquid nitrogen and placed on the ventricular surface until thawing could be observed (a few seconds). An Armaflex cover (Armacell, Germany) was used to protect cooling of the polypropylene tube. Sham operations consisted of touching the exposed ventricular surface with a copper filament at room temperature. After the operation, fish were placed in a tank of fresh water, and reanimation was enhanced by pipetting water onto the gills for a couple of minutes. Fish were swimming normally after half an hour. For analysis of regeneration, animals were killed at different times post-injury by immersion in 0.16% tricaine (Sigma, St Louis, MO, USA) and hearts were dissected in media containing 2 U/ml heparin and 0.1 M KCl. To assess the extent of damage caused by the procedure, photographs of cauterized hearts were taken between 1 and 24 hours post-injury. The damaged area was easily identified from the accumulation of blood at the injury site. Damage was also estimated by examination of sections, as previously described (Poss et al., 2002). The percentage of the ventricular surface area damaged by the procedure was calculated using Image J.

### Histological staining

Hearts were fixed in 4% paraformaldehyde (PFA) in phosphate-buffered saline (PBS) overnight at 4°C. Samples were then washed in PBS, dehydrated and paraffin wax embedded. Sections (7 μm) were cut on a Leica Microtome, mounted on Superfrost slides and dried overnight at 37°C. Sections were deparaffinized in xylol, rehydrated and washed in distilled water. Connective tissue was stained using the Masson-Goldner's trichrome procedure (Merk, Darmstadt, Germany). Muscle was stained brick red and connective tissue was stained green. As a more-sensitive assay for collagen deposition, sections were stained using the Picro-Mallory procedure. Muscle was stained light brown and collagen was stained blue.

### Immunofluorescence

Sections were deparaffinized, rehydrated and washed in distilled water. Epitopes were retrieved by heating in citrate buffer (pH 6.0) for 15 minutes in a microwave at full power. Non-specific binding sites were saturated by incubation for at least 1 hour in blocking solution (5% BSA, 10% goat serum, 0.3% Tween-20). Endogenous biotin was blocked with the avidin-biotin blocking kit (Vector, Burlingame, CA, USA). Primary antibodies used were anti-myosin heavy chain (MF20, DSHB), anti-tropomyosin (CH1, DSHB), anti-proliferating cell nuclear antigen (Santa Cruz Biotechnology, Santa Cruz, CA, USA), anti-myosin light chain kinase (Sigma, St Louis, MO, USA) and anti-GFP (Clontech, Mountain View, CA, USA). Biotin- or Alexa (488, 568, 633) -conjugated secondary antibodies (Invitrogen, Carlsbad, CA, USA) and streptavidin-Cy5 (Vector, Burlingame, CA, USA) were used to reveal primary antibody signal. Nuclei were stained with DAPI and slides were mounted in Vectashield (Vector, Burlingame, CA, USA). Apoptosis was detected by TUNEL staining using the in situ cell death detection kit from Roche (Mannheim, Germany).

### In situ hybridization on sections

In situ hybridization on paraffin sections was performed according to Mallo et al. with some modifications (Mallo et al., 2000).

### Imaging

Whole-heart images and videos were obtained with a Leica MZ16FA fluorescence stereomicroscope fitted with a Leica DFC310FX camera. A Nikon Eclipse 90i microscope was used for histological section imaging and a Leica TCS SP-5 confocal microscope for imaging immunohistochemical stains.

### Statistical analysis

Differences between mean proliferation values of experimental groups were tested for statistical significance by one-way ANOVA followed by Tukey's honest significant difference test to control for the multiplicity of the tests. Model assumptions of normality and homogeneity of variance were checked with conventional residual plots. We did not observe any strong deviation from normality or heterogeneity of variance that would justify the use of non-parametric tests. Data on ventricular hypertrophy were analyzed for statistical significance by two-tailed Student's *t*-test. Statistical significance was assigned at $P<0.05$.

## RESULTS

### Cryoinjury leads to scarring and subsequent clearance of the fibrotic tissue

In this article, we present a novel method that allows the study of heart regeneration in the zebrafish by inducing localized damage through cryocauterization (CC) of the ventricle. This system has been reported to be an alternative model to coronary artery ligation in mice (van den Bos et al., 2005) and is being used in the clinic as an ablative technique in the surgical treatment of arrhythmias (Gallagher et al., 1977; Watanabe et al., 1996). The pericardial cavity was opened in anesthetized animals and the ventricle was damaged at its ventral apex by the placing of a copper filament previously cooled in liquid nitrogen (for a detailed description see the Materials and methods). To monitor the induced damage and subsequent regeneration process, we performed Masson-Goldner trichrome histological staining on CC hearts at successive intervals after the induction of damage. At one day post-injury (dpi) the injured area (IA) occupied ~25% of the ventricular volume (Fig. 1A,A′) ($n$=6; mean±s.d.=24.4±7.9). Blood accumulated at the IA (Fig. 1A′). Damage to the myocardium in the IA reached its full extent at 3 dpi (Fig. 1B,B′). On the heart surface, particularly at the borders of the IA, an enlarged epicardial layer was detected during the first days after injury. Accumulation of a fibrotic scar in the IA was observed at this stage, visible as a green stain by Masson-Goldner trichrome histology (Fig. 1B). Fibrotic tissue persisted at

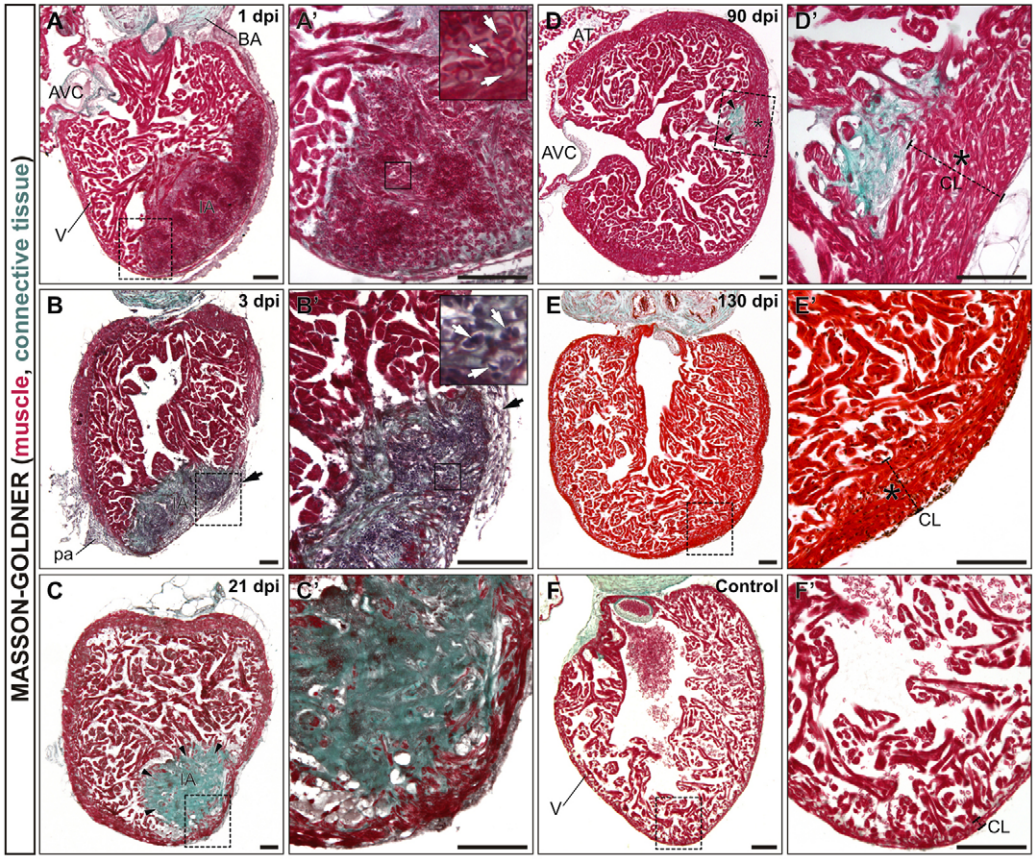


**Fig. 1. Complete regeneration and scar removal after cryoinjury of the adult zebrafish ventricle.** Masson-Goldner-Trichrome stained sagittal sections of adult zebrafish heart fixed at the indicated days after cryocauterization of 25% of the ventricular apex. Anterior is towards the top, ventral towards the right. Boxed areas of the cauterized region are shown at higher magnification in A′-F′. The staining reveals deposition of connective tissue and fibrotic areas in green and healthy myocardial tissue in red. (**A**,**A′**) At 1 dpi, there is still some trabeculated myocardium in the injured area (IA). Erythrocytes accumulate at the IA (white arrows in inset). (**B**,**B′**) Extensive fibrosis is visible at the IA at 3 dpi. The myocardium has been degraded by this stage. Note the infiltration of the IA with inflammatory cells (white arrows in inset). Black arrows in B and B′ indicate the thickened epicardial layer at 3 dpi. (**C**,**C′**) At 21 dpi the compact layer has regenerated and the IA is positioned at a more luminal region. (**D**,**D′**) Only a small remnant of the IA is visible at 90 dpi, positioned at the border between compact and trabeculated layers. (**E**,**E′**) At 130 dpi, regeneration is complete. Note the enlarged myocardial compact layer near the injury site at 90 dpi (D,D′, asterisk) and 130 dpi (E,E′, asterisk) compared with the control situation (**F**,**F′**). Arrows in all panels indicate fibrotic tissue accumulation. AT, atrium; AVC, atrioventricular channel; BA, bulbus arteriosus; CL, compact layer; dpi, days post-injury; IA, injured area; pa, pericardial adhesions; V, ventricle. Scale bars: 100 µm.

21 dpi (Fig. 1C,C′), although the affected area had shrunk by this stage. Notably, the scar was at a more luminal position, and the compact layer and part of the trabeculated layer had regenerated to surround the remaining scar. At 90 dpi, a remnant of the scar could still be detected in the trabeculated area of the ventricular apex, presumably at the site where the injury had been performed (Fig. 1D,D′) ($n$=6). At 130 dpi the scar had almost completely disappeared ($n$=4) (Fig. 1E,E′). The newly formed compact layer was particularly thick at the injury site (Fig. 1D,E). Comparison of the compact layers of cauterized and control hearts suggested that the compact layer of CC hearts was enlarged, and did not regain its normal thickness, even after long-term recovery (Fig. 1E-F′). Quantification revealed that the compact layer of the ventral ventricular apex was around twofold thicker than the contralateral (non-injured) side at 60 to 130 dpi ($n$=9; $P$<0.005).

To determine the dynamics of collagen deposition and removal after ventricular cryocauterization, and to compare this to the response to ventricular apex resection (VR), we performed Picro-Mallory staining at successive intervals after each procedure (Fig. 2). After CC, strong collagen deposition was visible at 7 dpi (blue stain) (Fig. 2A,A′). This was gradually eliminated during regeneration (Fig. 2B,B′), but persisted until late post-injury stages (Fig. 2C,C′). By contrast, resected hearts revealed less collagen deposition at 7 days post-amputation (dpa) (Fig. 2D,D′) and 21 dpa (Fig. 2E,E′). At late stages post-amputation, no collagen deposition could be observed, revealing a faster elimination of fibrotic tissue (Fig. 2F,F′).

We next determined the cellular composition of the fibrotic tissue by analyzing the expression of myosin light chain kinase (Mlck), a marker of smooth muscle cells, myofibroblasts and activated thrombocytes (Grimes et al., 2006; Tournoij et al., 2010). Mlck-positive cells accumulated at the IA border at 1 dpi (Fig. 3A,A′), suggesting the presence of activated thrombocytes. No Mlck-positive cells were detected within the IA at this stage (Fig. 3A′). At 3 dpi, Mlck-positive cells were found within the IA (Fig. 3B,B′), which at this stage is easy to identify by the lack of tropomyosin staining. The number of Mlck-positive cells increased by 21 dpi, suggesting the maturation of a smooth muscle-containing scar (Fig. 3C,C′). The number of Mlck-positive cells declined at later stages of regeneration. Only a few

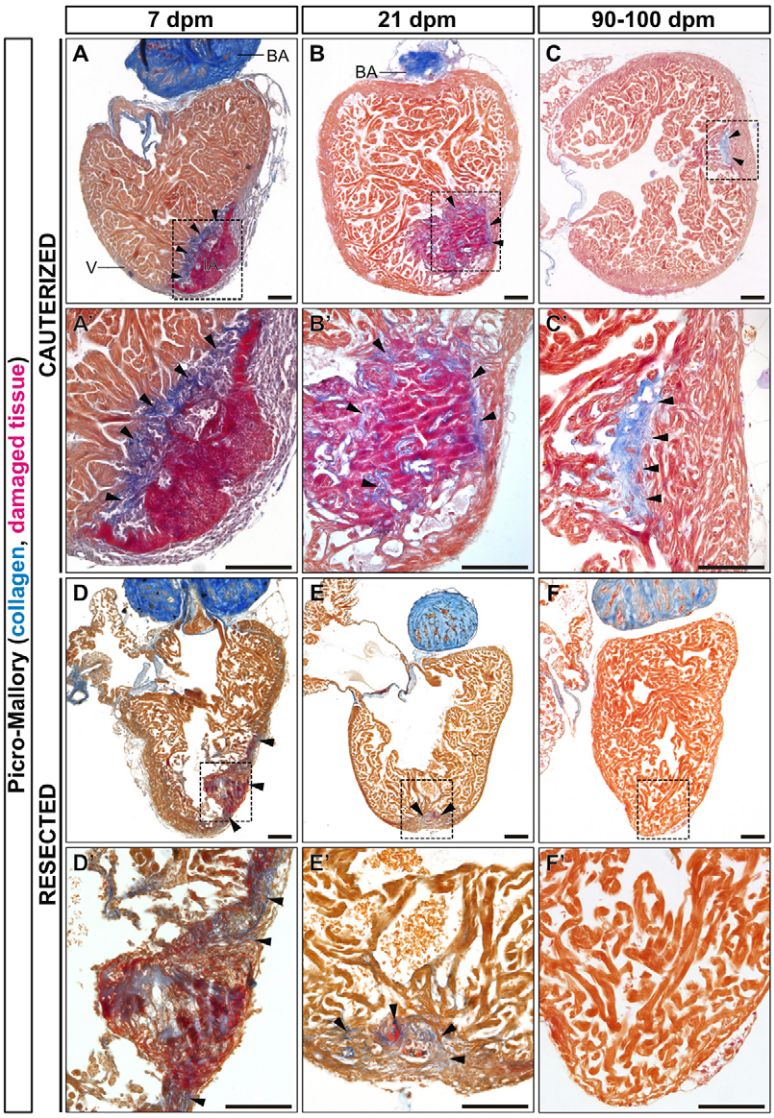


**Fig. 2. Comparison of collagen deposition and removal dynamics in cauterized and resected hearts.** (**A-F**) Picro-Mallory stained sagittal sections of adult zebrafish heart fixed at the indicated days after cryocauterization (A-C) or resection (D-F) of the ventricular apex. Collagen is stained blue, damaged tissue in red and myocardium in brown. (**A′-F′**) Boxed areas of the damaged region shown at higher magnification. Anterior is towards the top, ventral towards the right. The strong collagen staining at the bulbus arteriosus acts as a positive control. (A-C′) Massive collagen deposition can be observed upon cauterization, which persists until late stages, indicating the formation of a scar. (D-F′) Resection triggers less collagen deposition than observed upon cryoinjury. Although a collagen scar persists until late stages after cauterization (C), it completely disappears after resection (F,F′). Arrowheads indicate sites of collagen deposition. BA, bulbus arteriosus; dpa, days post-amputation; dpi, days post-injury; IA, injured area; V, ventricle. Scale bars: 100 μm.

Mlck-positive fibers were found at 90 dpi (Fig. 3D,D′), suggesting the gradual elimination of the cellular components of the fibrotic tissue.

Cryocauterization of the zebrafish heart thus leads to the destruction of 25% of the ventricle, and the formation of a massive scar appears to be compatible with cardiac regeneration. In contrast to the situation in mammals, this scar is gradually reabsorbed during regeneration. This process includes the removal of both the cellular and the acellular scar components, as revealed by the progressive loss of Mlck-positive cells and histological stains. However, some fibrosis persists even after long-term recovery.

## Cryoinjury induces apoptosis of cardiac tissue

To address the effect of CC on heart apoptosis in the zebrafish we performed TUNEL (TdT-mediated nick end labeling) staining on the hearts of Tg(*fli1a:GFP*) transgenic zebrafish, in which the promoter of the endothelial marker *fli1a* drives the expression of GFP in the coronary vessels and endocardium (Lawson and Weinstein, 2002). Control hearts were almost devoid of TUNEL-positive cells (Fig. 4A), whereas sham-operated hearts contained a few apoptotic cells 4 hours after operation (Fig. 4B). By contrast, massive cell death was found at the injury site 4 hours post-injury (hpi) (Fig. 4C). Apoptotic cells also accumulated in the vascular lumen of coronary vessels in the periphery of the IA, indicating that CC causes cell death in the vasculature beyond the IA (Fig. 4C,G,G′″). In hearts damaged by VR, we detected accumulation of apoptotic cells at the borders of the resected area but not elsewhere (Fig. 4D). To study the distribution of apoptotic cells in more detail, TUNEL detection was repeated on heart sections at different intervals after injury. Control and sham-operated hearts contained few apoptotic cells (Fig. 4E,E′,F,F′). Although tropomyosin staining in the IA was indistinguishable from that in the rest of the heart at 4 hpi, massive TUNEL staining is visible at the IA (Fig. 4G). Note that DAPI staining was nearly absent in the IA, probably as a consequence of nuclear fragmentation (Fig. 4G). A higher magnification view confirmed the presence of enucleated cardiomyocytes in the IA (see Fig. S1 in the supplementary material). TUNEL-positive pyknotic nuclei could be found in cardiomyocytes and endocardial cells within the IA (Fig. 4G′,G″ and see Fig. S2A-B‴ in the supplementary material). Confirming the analysis in whole-mount hearts, sagittal sections revealed TUNEL-positive vascular endothelial cells in the IA periphery (Fig. 4G‴ and see Fig. S2C-C‴ in the supplementary material). Cell death declined over subsequent days (Fig. 4H-I′): apoptotic cells

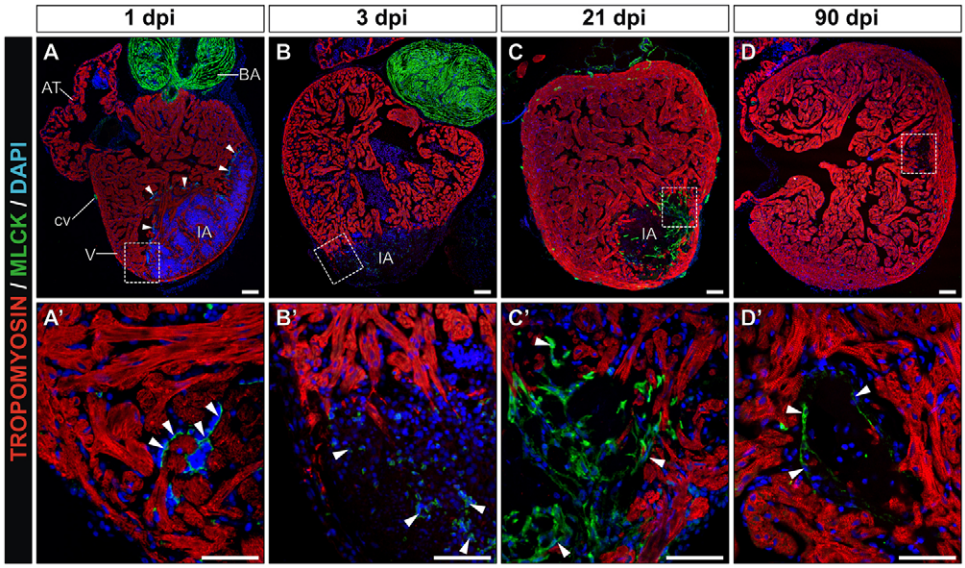


**Fig. 3. Cryocauterization-induced myofibroblast accumulation and subsequent elimination during scar removal.** (**A-D**) Immunohistochemistry on sagittal sections of cauterized hearts on the indicated days post-injury with antibodies to tropomyosin (red) and myosin light chain kinase (Mlck) (green); nuclei are stained with DAPI (blue). Anterior is towards the top, ventral towards the right. (**A′-D′**) Higher magnification views of the boxed areas in A-D. Arrowheads indicate Mlck-positive cells. (A,A′) Note the accumulation of Mlck at the borders of the injured region at 1 dpi, revealing activated thrombocytes. (B,B′) At 3 dpi, some Mlck-positive cells appear at the injury site. (C,C′) At 21 dpi, a Mlck-positive scar has formed, which partially persists until late stages of regeneration. (D,D′) At 90 dpi, only a few Mlck-positive cells can be detected in the scarred region. AT, atrium; BA, bulbus arteriosus; cv, coronary vessel; dpi, days post-injury; IA, injured area; V, ventricle. Scale bars: 100 µm.

were only rarely found in hearts at 3 dpi (Fig. 4H′) and 21 dpi (Fig. 4I′). At these stages, apoptotic cells were restricted to the IA or the IA borders, suggesting that the dying cells might be inflammatory cells (Fig. 4H″,I″).

## Cardiac tissue regeneration after cryoinjury

To better understand the regeneration of the different cell types that comprise the heart, we monitored post-CC recovery in the Tg(*fli1a:GFP*) endothelial reporter line (Lawson and Weinstein, 2002) and the Tg(*cmcl2:GFP*) myocardial reporter line, which expresses GFP under the control of cardiac myosin light chain 2 promoter. At 1 hpi, cauterized hearts had lost all blood vessels covering the IA (Fig. 5A). This was followed, however, by rapid regeneration of the coronary vasculature, with vessel sprouts already invading the IA at 3 dpi (Fig. 5B). At 21 dpi, the IA was almost completely covered by coronary vasculature (Fig. 5C), and from 40 dpi onwards GFP expression in cauterized and control Tg(*fli1a:GFP*) hearts was indistinguishable in whole-mount view (Fig. 5D,E).

In Tg(*cmcl2:GFP*) hearts at 1 hpi to 3 dpi, the IA was completely devoid of GFP expression (Fig. 5F,G). GFP expression gradually recovered, during subsequent stages of regeneration (Fig. 5H). We did not detect GFP inside the IA, but observed that the GFP-negative area became progressively smaller over the following weeks, suggesting that newly formed cardiomyocytes are added from the border zone of the IA during the regeneration process. At 90 dpi there was no observable difference in GFP expression between cauterized and control hearts in whole-mount view (Fig. 5I,J).

Myocardial injury triggers the reactivation of epicardial marker genes (Lepilina et al., 2006; Limana et al., 2009). Indeed, at least in the zebrafish, this reactivation also occurs as a response to changes in pericardial fluid osmolarity (Wills et al., 2008). We analyzed the response of the epicardial layer to cryocauterization in the Tg(*wt1b:GFP*) line (Perner et al., 2007). To validate the use of the Tg(*wt1b:GFP*) line as an epicardial reporter line, we compared expression of GFP with the expression of the epicardial marker genes *wt1b* and *wt1a* by in situ hybridization on adjacent sections (Perner et al., 2007; Serluca, 2008) (see Fig. S3 in the supplementary material). In cauterized hearts at 3 dpi, *wt1a*- and *wt1b*-positive cells were detected in the epicardium, but expression of *wt1b* covered a larger area (see Fig. S2A,B in the supplementary material). The expression pattern of *GFP* correlated with the *wt1b* mRNA expression in Tg(*wt1b:GFP*) hearts (see Fig. S2C in the supplementary material). Thus, GFP expression in this line recapitulates expression of an endogenous epicardial marker gene. Injured and sham-operated hearts revealed a strong upregulation of GFP expression on the heart surface already visible at 1 dpi (Fig. 5K,P). GFP-positive cells were often found close to coronary vessels. Pericardial adhesions also showed high GFP expression (Fig. 5K). In cauterized hearts, GFP expression remained high over the weeks following injury (Fig. 5L-N). Expression was particularly intense at the border of the IA and in a subset of epicardial cells close to the coronary vessels. Even at the latest stage analyzed (90 dpi), a patch of GFP expression could be observed at the ventricular apex, coinciding with the region of induced damage (Fig. 5N). Thus, the elevated GFP expression in cauterized hearts is sustained. By contrast, GFP expression declined to basal levels by 21 dpm in sham-operated hearts (Fig. 5Q-S). In non-operated Tg(*wt1b:GFP*) fish, GFP expression in the heart was detected only at basal level in a few cells on the ventricular surface, bulbus arteriosus and atrium, in many cases surrounding coronary vessels or associated with epicardial adipose tissue (Fig. 5O,O′).

Although the recovery of myocardium and coronary vasculature was complete, the shape of post-cauterized ventricles differed from that of control hearts. The regenerated area ballooned out, giving the

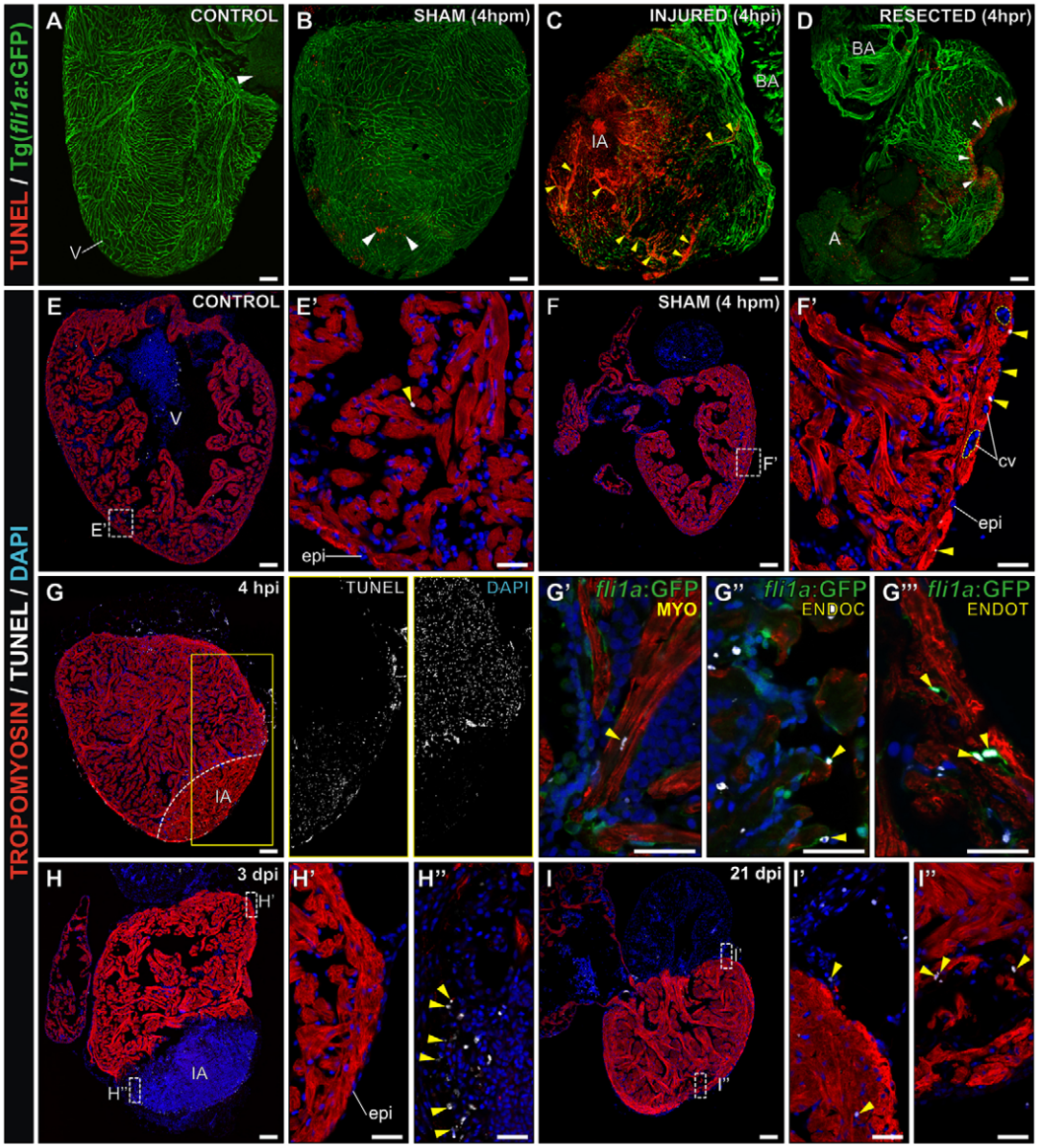


**Fig. 4. Cryocauterization induces extensive cardiac apoptosis.** (**A-D**) Confocal 3D projections of whole-heart TUNEL staining of Tg(*fli1a*:GFP) zebrafish, in which the endocardium and vascular endothelium are revealed by GFP immunohistochemistry. White arrowheads indicate TUNEL-positive cells. (A) Untreated (control) heart revealing few TUNEL-positive cells. (B) Sham-operated heart, revealing a slight increase in apoptosis in response to pericardial sac rupture at 4 hours post-manipulation (4 hpm). (C) Cryocauterized heart. Massive cell death is evident at the injury site and also in the vascular lumen of coronary vessels far from the injured area at 4 hours post-injury (4 hpi). Yellow arrowheads indicate TUNEL-positive capillaries. (D) Resected heart. Ventricular resection provokes apoptosis in a small area close to the amputation plane. (**E-I″**) TUNEL staining (white) and immunohistochemistry against tropomyosin (red) and GFP (green) on sagittal heart sections. Nuclei are stained with DAPI (blue). Yellow arrowheads indicate TUNEL-positive cells. (E,E′) Few apoptotic cells are detected in control hearts. (F,F′) In sham-operated hearts at 4 hpm, increased numbers of apoptotic cells are observed in the epicardium but not in the coronary vessels (F′, highlighted with broken lines). (G-G‴) In cryocauterized hearts at 4 hpi, extensive cell death is visible at the injury site (compare adjacent panels in G showing greyscale images of TUNEL and DAPI stainings). Although tropomyosin staining is still present in the injured area (IA), DAPI and TUNEL staining reveal that these are enucleated cardiomyocytes undergoing cell death. (G′-G‴) Higher magnification views of the boxed area in G, revealing a TUNEL-positive cardiomyocyte in the IA (G′), TUNEL-positive endocardial cells in the IA (G″) and TUNEL-positive vascular endothelial cell nuclei in the proximity of the IA (G‴). (H-H″) At 3 dpi, apoptosis decreased in coronary endothelial cells and epicardium of the periphery (H′), while apoptotic cells can be found within the IA (H″). (I-I″) At 21 dpi apoptosis has generally decreased (I′) and apoptotic cells concentrate at the IA borders (I″). A, atrium; BA, bulbus arteriosus; dpm, days post-manipulation; dpi, days post-injury; epi, epicardium; hpm, hours post-manipulation; hpi, hours post-injury; hpr, hours post-resection; IA, injured area; V, ventricle. Anterior is towards the top, ventral towards the right in all panels. Scale bars: general view, 100 μm; higher magnification views, 25 μm.

heart a rounder shape (compare Fig. 5D with 5E and Fig. 5I with 5J). These shape differences suggest altered cardiac function, and analysis of ventricular contraction in CC hearts at 130 dpi detected irregular ventricular contraction, in which the ventral part of the ventricle revealed limited contractability ($n$=4 out of 4; see Movies 1 and 2 in the supplementary material). Cardiac tissues thus regenerate after cryoinjury but functional recovery of the heart is probably incomplete.

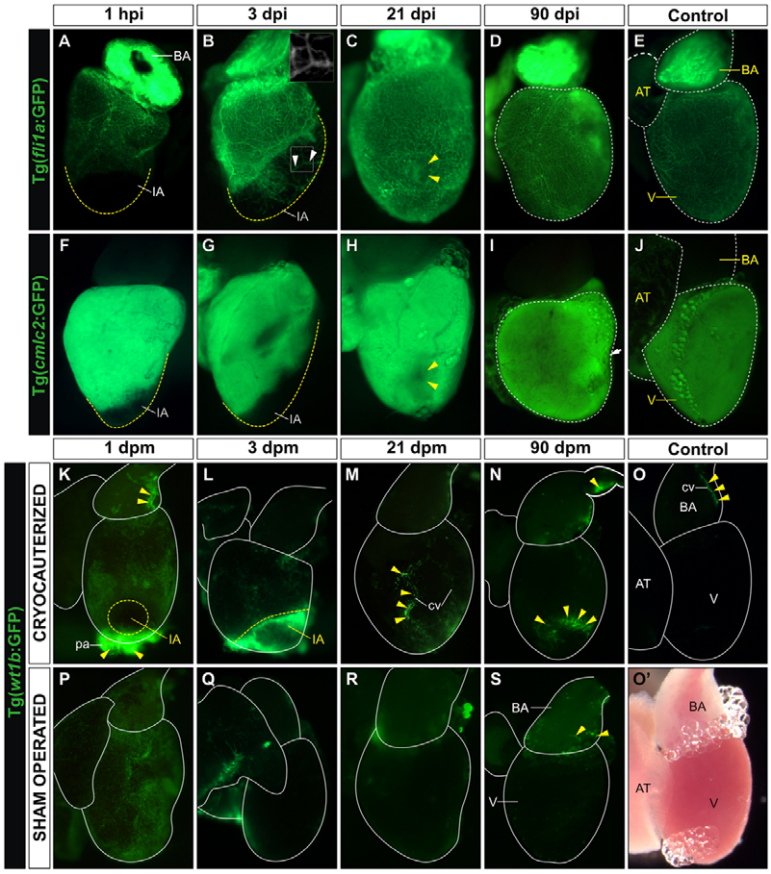


**Fig. 5. Cardiac tissue regeneration upon cryocauterization.** (A-D,F-I) Whole-mount views of dissected hearts of Tg(*fli1a:GFP*) zebrafish (indicating endocardium and vascular endothelium; A-D) and Tg(*cmlc2:GFP*) zebrafish (indicating myocardium; F-I) at the indicated times post-injury (hpi or dpi). (E,J) Untreated controls. Anterior is towards the top, ventral towards the right. Broken yellow lines demark the injured area (IA) or the nonregenerated remnant of the IA. (**A**) Upon cryoinjury, the coronary vasculature and endocardium are completely devoid of GFP expression. (**B**) At 3 dpi, the IA becomes vascularized (indicated by arrowheads and highlighted in inset box). (**C**) At 21 dpi, the IA (yellow arrowheads) is nearly indistinguishable from surrounding tissue. (**D**) By 90 dpi, GFP expression in cryoinjured hearts is similar to control Tg(*fli1a:GFP*) hearts. (**F**,**G**) Lack of myocardial GFP expression in the IA after cryocauterization. (**H**) Recovery of myocardial GFP expression at 21 dpi; note the small GFP-negative region in the myocardium (yellow arrowheads), possibly a remnant of the IA. (**I**) By 90 dpi, myocardial GFP expression in cryoinjured hearts is similar to that in control Tg(*cmlc2:GFP*) hearts. The arrow and broken lines in D and I indicate major long-term morphological alterations in ventricular shape after injury, compared with controls (**E**,**J**). (K-S) Whole-mount views of dissected hearts of Tg(*wt1b:GFP*) zebrafish (indicating epicardium) in cryocauterized hearts (K-N), control hearts (O,O′) and sham-operated hearts (P-S). Yellow arrowheads mark sites of GFP expression. (**K**) Upon injury, GFP expression is activated on the surface of the heart and pericardium. (**L**) Expression remains high at 3 dpi, especially close to the IA. (**M**,**N**) GFP expression is downregulated at later stages but is still visible at the borders of the IA and in association with coronary vessels. (**O**) Non-injured control heart revealing just a few GFP-positive cells in the bulbus arteriosus. (**O′**) Bright-field image of the same heart as in O. (**P**) Sham-operated heart revealing GFP expression in the epicardium. (**Q-S**) At 3 dpm, GFP expression is already downregulated and remains low at all later stages analyzed. AT, atrium; BA, bulbus arteriosus; cv, coronary vessel; IA, injured area; V, ventricle.

## Proliferative response to cryoinjury

We next analyzed the capacity of CC to induce proliferative responses in vascular endothelial cells, endocardial, myocardial and epicardial cells by staining for proliferating cell nuclear antigen (PCNA) (Figs 6 and 7). Staining of sagittal sections of Tg(*fli1a:GFP*) hearts revealed little cell proliferation in the hearts of control zebrafish kept under standard conditions (Fig. 6A,A′), and proliferation was not increased significantly by opening of the pericardial sac (Fig. 6B,B′,E-G). By contrast, significant proliferation was detected in heart tissue in the days immediately following CC in all cell types analyzed.

Vascular endothelial cell proliferation was not restricted to the injury site but was also detected in the periphery, suggesting a paracrine induction of angiogenesis (Fig. 6C,C′,E). The proliferative response to CC injury was also detected in the endocardial layer (Fig. 6C,C″). At 3 dpi, most endocardial cells at the injury border were proliferating, and newly formed endocardium could be observed protruding into the injury site (Fig. 6C″,F). Cardiomyocyte proliferation peaked during the first week after cauterization. Whereas the hearts of control and sham-operated animals contained minor scattering of proliferating cardiomyocytes (Fig. 6A-B′), these cells were much more abundant throughout the CC heart (Fig. 6C, C′,G) particularly at the injury border zone in both the trabeculated and compact myocardium (Fig. 6C″,C‴,G). Proliferation in myocardium, endocardium and coronary vasculature decreased at later stages, with few proliferating cells detected in CC hearts by 21 dpi (Fig. 6D-D″).

The massive expansion of the epicardial layer observed on histological stainings of cryoinjured hearts was confirmed by immunohistochemistry on sagittal heart sections of Tg(*wt1b:GFP*)

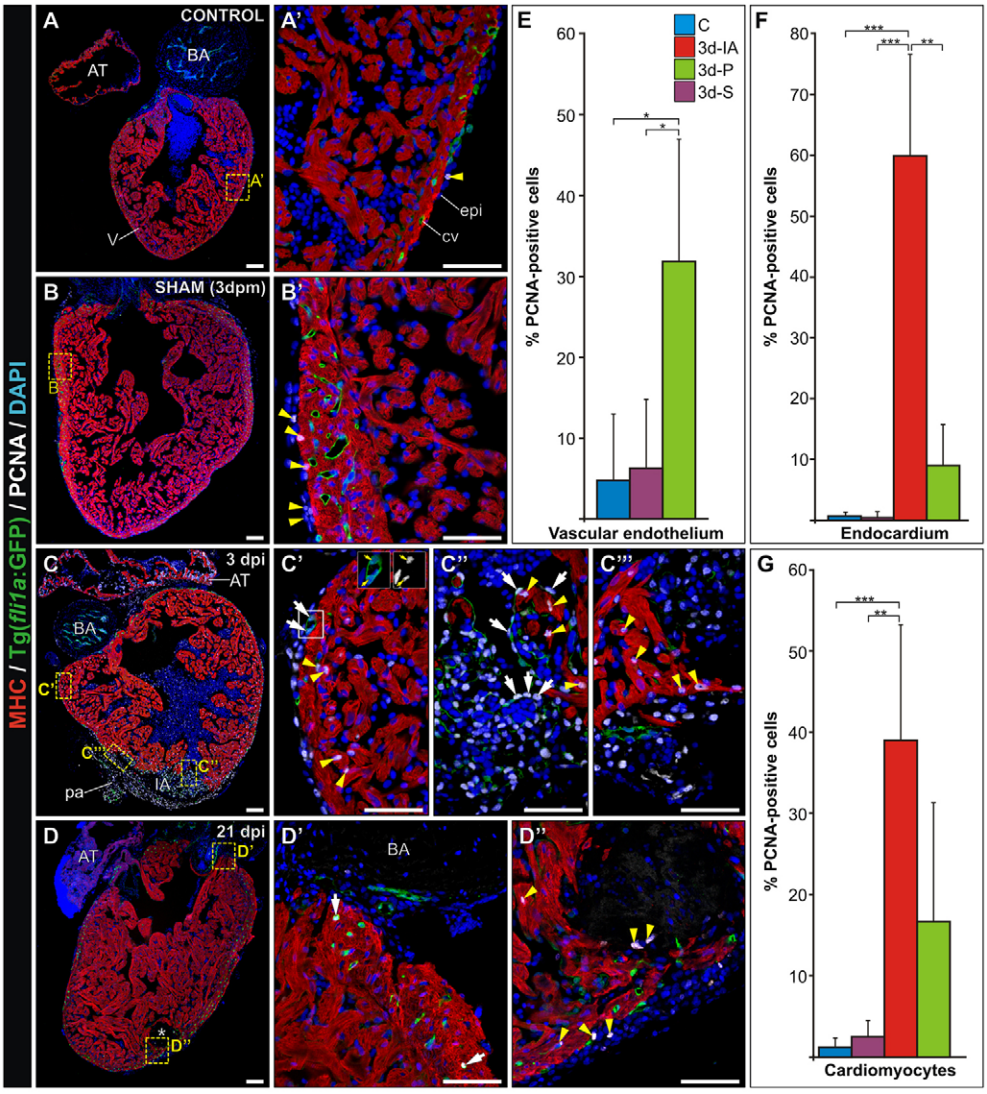


**Fig. 6. Ventricular cryocauterization induces a proliferative response in cardiac cells.** Immunostaining of sagittal Tg(*fli1a:GFP)* heart sections for myosin heavy chain (MHC, red), GFP (green) and proliferating cell nuclear antigen (PCNA; white). Nuclei are stained with DAPI (blue). Proliferating (PCNA-positive) cells are indicated with yellow arrowheads. Anterior is towards the top, ventral towards the right. (**A**,**A′**) Untreated (control) heart revealing few proliferating cells. (**B**,**B′**) Sham-operated heart; pericardial sac opening leads to a limited increase in cell proliferation in the epicardium. (**C**-**C‴**) Cryoinjured heart at 3 dpi. (C′) Extensive proliferation is detected away from the injured area (IA) in epicardium, cardiomyocytes and endocardial cells. White arrows indicate proliferating vascular endothelium. Inset shows a detailed view of proliferating endothelial cells (yellow arrows indicate PCNA-positive nuclei). (C″) In the trabeculated myocardium bordering the IA, both cardiomyocytes (yellow arrowheads) and endocardial cells (white arrows) are highly proliferating. (C‴) PCNA-positive cardiomyocytes in the compact layer are indicated by yellow arrowheads. (**D**) Cryoinjured heart at 21 dpi. Asterisk indicates the IA. (**D′**) Only a few proliferating cells are detected in the periphery (white arrows indicate coronary endothelial cells). (**D″**) Few proliferating cells (yellow arrowheads) are found close to the IA. (**E-G**) Quantification of proliferating vascular endothelial cells, endocardial cells and cardiomyocytes in control (C), sham-operated (3d-S) and cauterized hearts at regions close to (3d-IA) or distant from (3d-P) the injured area at 3 dpm. For each condition, PCNA-positive cells were counted in three to five hearts (at least two sections per heart). Data are mean±s.d.; **P*<0.05; ***P*<0.01; ****P*<0.001 (one-way ANOVA followed by Tukey's honest significant difference test). AT, atrium; BA, bulbus arteriosus; cv, coronary vessel; dpm, days post-manipulation; dpi, days post-injury; epi, epicardium; IA, injured area; pa, pericardial adhesion. Scale bars: general view, 100 μm; higher magnification views, 50 μm.

fish. The epicardium of control hearts was almost devoid of GFP-positive cells (Fig. 7A,A′) and none was found to be proliferating (*n*=3 analyzed hearts). Epicardial GFP expression was rapidly upregulated after sham-operation (Fig. 7B,B′), but few of these epicardial cells were proliferating (Fig. 7D″). The presence of GFP-positive cells in the epicardial layer persisted until around 3 weeks pm and was downregulated at later stages (Fig. 7C,C′ and not shown). By contrast, CC hearts revealed a massive increase in proliferation of wt1b:GFP-positive cells (Fig. 7D,D′). At 3 dpi, more than 70% of epicardial GFP-positive cells were co-labeled with PCNA (Fig. 7D′). This increased proliferation led to an expansion of the epicardial layer from the usual single cell layer to a multilayered epicardial sheet more than five cells deep (Fig. 7D,D′). The epicardial layer was especially thick at the injury site, forming a cap covering the IA. Over the following days this layer thinned and compacted (Fig. 7E-F′), returning to its normal one-cell thickness by 3-4 weeks post-injury

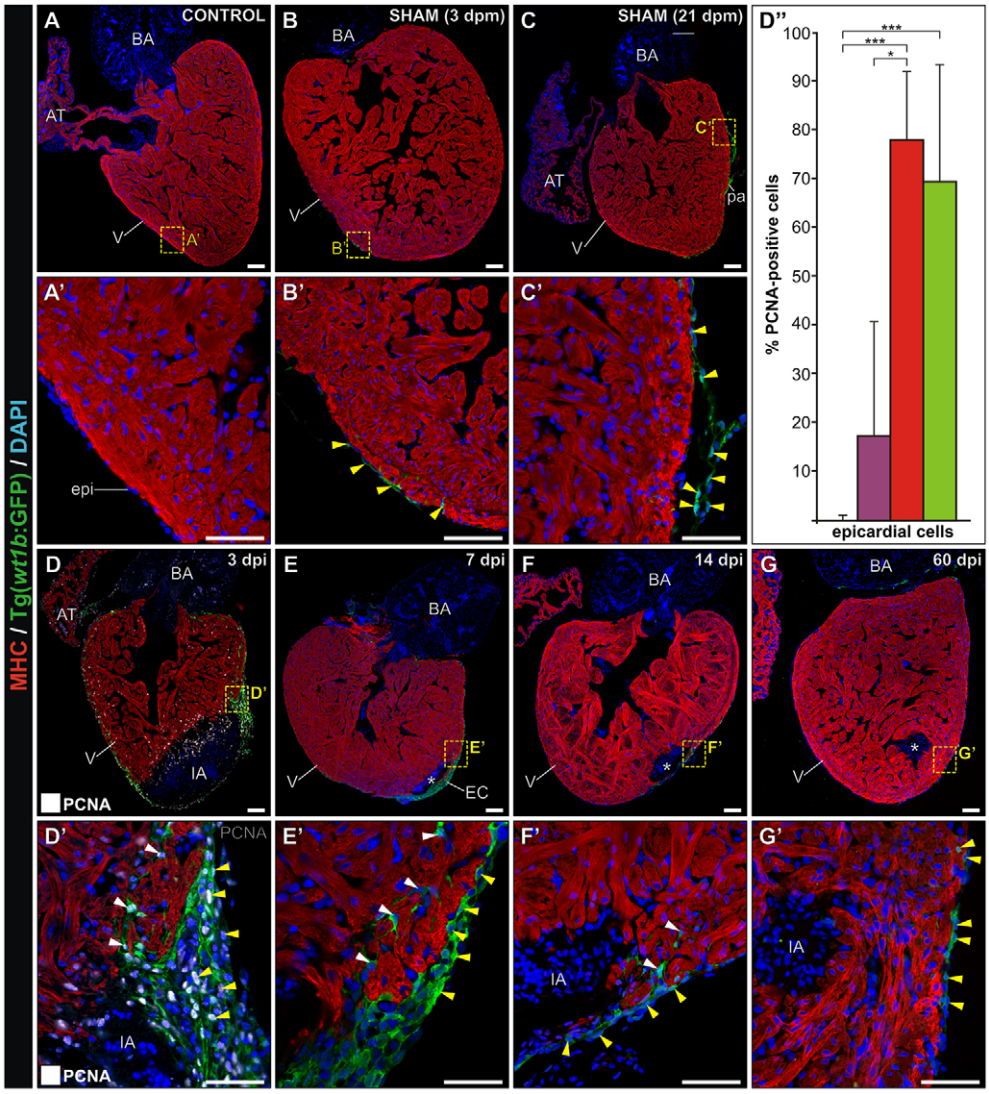


**Fig. 7. Ventricular cryocauterization induces a proliferative response in epicardial cells.** Immunostaining of sagittal Tg(*wt1b:GFP*) heart sections for myosin heavy chain (MHC) (red) and GFP (green). Nuclei are stained with DAPI (blue). Proliferating (PCNA-positive) cells are indicated with yellow arrowheads. Anterior is towards the top, ventral towards the right. Asterisks indicate the injured area (IA). Yellow arrowheads indicate GFP-positive cells in the epicardium. White arrowheads indicate GFP-positive cells in the compact layer. (**A**,**A′**) Untreated (control) heart revealing no GFP-positive cells. (**B**,**B′**) Sham-operated heart at 3 dpm; pericardial sac opening leads to GFP expression in epicardial cells. (**C**,**C′**) At 21 dpm, some GFP-positive cells are found in the epicardium. (**D**,**D′**) Cryoinjured heart at 3 dpi; proliferating (PCNA-positive) cells are shown white. Extensive proliferation is detected in the epicardium, especially at the borders of the IA. (D′) Nearly all GFP-positive cells are proliferating at this stage. The epicardial layer is several cell diameters thick. GFP-positive cells can also be found protruding into the compact layer. (**D″**) Quantification of proliferating epicardial cells in control sham-operated (violet) and cauterized hearts at regions close to (red) or distant from (green) the injured area at 3 dpm. For each condition, PCNA-positive cells were counted in three to five hearts (at least two sections per heart). Data are mean±s.d.; $^{**}P<0.01$; $^{***}P<0.001$ (one-way ANOVA followed by Tukey's honest significant difference test). (**E**,**E′**) At 7 dpi, GFP-positive epicardial cells cover the IA. (**F**,**F′**) Cryoinjured heart at 14 dpi; note the reduced thickness of the epicardial cap compared with earlier stages. (**G**,**G′**) Cryoinjured heart at 60 dpi. GFP-positive cells can also be found covering the remnants of the IA, although the epicardial layer has returned to its normal thickness of one cell diameter. AT, atrium; BA, bulbus arteriosus; dpi, days post-injury; dpm, days post-manipulation; epi, epicardium; IA, injured area; pa, pericardial adhesion. Scale bars: general view, 100 μm; higher magnification views, 50 μm.

(Fig. 7G,G′). Although GFP expression was mostly found in the epicardium, some GFP-positive cells with visible cellular protrusions were found in the compact layer of the heart (Fig. 7D′,E′,F′).

## DISCUSSION

### Cell responses during cardiac regeneration after cryoinjury

The results presented here show that the adult zebrafish heart is able to completely regenerate after cryocauterization (CC). CC of 25% of the zebrafish ventricle is followed by complete regeneration of myocardium, endocardium and coronary vasculature. Regeneration in CC occurs over a longer timeframe than in VR, even though a similar amount of heart tissue is lost in both models. This delay probably reflects the need to remove necrotic tissue after CC before regeneration of the damaged area can occur.

Apart from the overt necrosis, myocardial infarction in mammals also leads to myocardial cell death by apoptosis. Similar to what can be found following ischemic insults in mammals, dead cardiomyocytes show cytoplasm positive for

contractile proteins and absence of nuclei at few hours post-cauterization of the zebrafish heart. The apoptosis in the myocardium of cryoinjured zebrafish hearts is thus similar to the cell death observed in myocardial infarction models in mammals (Itoh et al., 1995; Saraste et al., 1997). Apoptosis is triggered early after CC in the coronary vasculature, outside the borders of the IA, probably as a consequence of hypoxia induced by blood flow interruption. Cauterization thus seems to lead to a more widespread and severe vascular apoptosis than is triggered by VR. During subsequent regeneration, proliferating vascular endothelial cells are found throughout the heart. Although we cannot rule out revascularization through vasculogenesis, we did not detect individual *fli:*GFP-positive angioblast precursor cells scattered over the IA, which would suggest the eventual formation of a new vascular plexus. Instead, we detected capillaries sprouting from the border zones and invading the IA, suggesting directed migration towards the damaged tissue. Thus, angiogenesis seems to be fundamental to the restoration of the interrupted blood flow.

*wt1b* is expressed during epicardial development (Perner et al., 2007; data not shown) and its re-expression in the adult zebrafish epicardium upon CC, which was also observed in the Tg(*wt1b:GFP*) reporter line, is consistent with the previously described re-expression of developmentally active genes upon cardiac damage (Lepilina et al., 2006; Limana et al., 2007; Wagner et al., 2002). At early time points after injury, the epicardium thus shows a systemic response to injury. Interestingly, the epicardial response partially persists for at least 3 months. We not only observed an upregulation of epicardial genes, but also a massive epicardial proliferation that might indicate a need to cover the damaged area. During development, the epicardium has been shown to stimulate myocardial cell proliferation through the secretion of trophic factors (Sucov et al., 2009). Therefore, the increased epicardial population might act as a source of signaling molecules that drives regeneration of the underlying myocardium.

During development, EPDCs give rise to vascular smooth muscle cells, fibroblasts and, in the chick and to a lesser extent in the mouse, to vascular endothelial cells (Gonzalez-Rosa et al., 2010; Lie-Venema et al., 2007; Smart et al., 2009). Thus, during regeneration, EPDCs might serve as a progenitor cell source to repopulate the damaged heart. EMT in the epicardium has recently been described to occur as well during regeneration (Kim et al., 2010). Thus, the small population of wt1b:GFP cells in the compact layer might derive from EPDC that delaminated from the epicardium and migrated into the myocardium. Transplantation of human EPDCs into a mouse heart after coronary artery occlusion results in improved cardiac function, demonstrating that EPDCs have a genuine therapeutic potential to restore heart function after MI (Winter et al., 2007). The potential of ectopic factors to promote EPDC migration or proliferation is currently under investigation. For example, administration of the signaling molecule thymosin β4 enhances epicardial marker gene expression and slightly improves capillary formation at the infarction border zone in adult mice following coronary artery ligation (Bock-Marquette et al., 2009). In this regard, the zebrafish is an appropriate model organism for pharmacological screening of novel molecules with epicardial cell activating potential.

During the formation of the new compact layer, the most central part is the last to be formed, suggesting that regeneration occurs from the periphery towards the center of the damaged area. The increased myocardial proliferation at the IA border in the zebrafish CC model supports the idea that during zebrafish cardiac regeneration the newly formed myocardium derives from pre-existing cardiomyocytes close to the injury site (Jopling et al., 2010; Kikuchi et al., 2010). We detected high levels of cardiomyocyte proliferation in both the compact layer (CL) and the trabeculated layer (TL). This suggests that the regenerated myocardium does not derive solely from a pre-existing subepicardial population in the CC model, as has been suggested for the VR model (Kikuchi et al., 2010). Instead, it appears that trabeculated and compact layers contribute equally to the repopulation of the damaged region. At 3 dpi, few CL cardiomyocytes appear at the border zone of the injury site in close apposition to the epicardial layer, which covers the injured region. CL cardiomyocytes seem to lag behind epicardial cells in the regeneration process, suggesting that the epicardium might serve as a scaffold for de novo formed cardiomyocytes. We also observed a previously unreported early endocardial proliferative response, suggesting that the newly formed endocardial layer serves as a scaffold for TL myocardial cells to replace the damaged tissue. Alternatively, these cells might exert a paracrine effect on myocardial cells, for example by secreting trophic factors necessary for their proliferation, or they might be a source of myofibroblasts, as has been reported in other species (Zeisberg et al., 2007), contributing to scar formation and removal. In summary, our results suggest that the epicardium in the CL and the endocardium in the TL exert paracrine and scaffolding effects on cardiomyocytes during regeneration.

## Cryocauterization as a model for the study of cardiac scar regression

Cardiac regeneration in zebrafish upon amputation of the ventricular apex has been extensively studied; however, there has been no description of heart regeneration in response to a lesion more similar to the pathophysiological condition of myocardial infarction, which involves tissue damage rather than tissue loss. One proposed alternative is genetic ablation of cell lineages (Curado et al., 2007). This approach is, however, restricted to a single cardiac cell type and is induced in the whole heart, and thus does not reproduce the localized damage that follows heart infarction.

Our findings suggest CC as an alternative model for the study of heart regeneration after myocardial damage in the zebrafish. As an IA is generated in this model, regeneration processes can be monitored and the interactions between healthy and injured tissues can be studied. Moreover, CC leads to the destruction of all cardiac cell types in a process that resembles the cardiac necrosis induced by MI in mammals. Although recent functional analysis of the regenerated heart after VR suggests a complete recovery of cardiac function, the regenerated heart after CC has notable morphological alterations, such as a rounded ventricular shape, thickened ventricular wall and arrhythmic ventricular contractions. These pathological alterations might be partially comparable with the ventricular remodeling that underlies some of the long-term consequences of mammalian heart infarction. Moreover, cryoablation is used for the correction of arrhythmias in humans (LaPage et al., 2010). Thus, CC in the zebrafish might represent a unique opportunity to investigate potential therapeutic strategies and reduce side effects of cryoablation in a simple vertebrate model.

Most importantly, a prominent collagen deposition lesion forms in the CC model that, compared with the lesion formed upon VR, better resembles the fibrotic scars formed after MI in mammals

(Yang et al., 2002). Recently, genetic inhibition of FGF signaling after VR in the zebrafish has been reported to induce irreversible scarring (Kikuchi et al., 2010). Interestingly, myocardial regeneration takes place even in the presence of this scar. Our present results support the notion that scarring does not inhibit cardiomyocyte proliferation during heart regeneration in the zebrafish. Moreover, our findings provide the first evidence that this scar is progressively removed in the zebrafish in a pathophysiological context, suggesting that scarring is reversible and that endogenous mechanisms of scar removal are present in this animal model. Thus, CC-induced injury in the zebrafish might provide important information with potential translational impact on post-MI management in humans.

**Acknowledgements**
We thank the CNIC animal facility and, in particular, Eduardo Díaz for excellent zebrafish husbandry. We are grateful to Enrique Lara-Pezzi and Ignacio Flores for comments on the manuscript, to Borja Ibañez for discussion on the cryoinjury technique, and to Simon Bartlett for text editing. Statistical analysis was performed with help from Pedro López. The Tg(*wt1b:GFP*) line was kindly provided by Christoph Englert (Fritz-Lipman Institute, Jena, Germany) and the Tg(*cmlc2:GFP*) line from Angel Raya (IBEC, Barcelona). MF20 and CH1 monoclonal antibodies were obtained from the Developmental Studies Hybridoma Bank developed under the auspices of the NICHD and maintained by The University of Iowa. Funding was from the Fundación Centro Nacional de Investigaciones Cardiovasculares Carlos III, the Fundación ProCNIC and the Spanish Ministry of Science and Innovation (FPU fellowship to J.M.G.-R., RYC-2006-001694 and BFU-2008-0012BMC to N.M.).

**Competing interests statement**
The authors declare no competing financial interests.

**Supplementary material**
Supplementary material for this article is available at
http://dev.biologists.org/lookup/suppl/doi:10.1242/dev.060897/-/DC1

**References**

**Bergmann, O., Bhardwaj, R. D., Bernard, S., Zdunek, S., Barnabe-Heider, F., Walsh, S., Zupicich, J., Alkass, K., Buchholz, B. A., Druid, H. et al.** (2009). Evidence for cardiomyocyte renewal in humans. *Science* **324**, 98-102.
**Bersell, K., Arab, S., Haring, B. and Kuhn, B.** (2009). Neuregulin1/ErbB4 signaling induces cardiomyocyte proliferation and repair of heart injury. *Cell* **138**, 257-270.
**Bock-Marquette, I., Shrivastava, S., Pipes, G. C., Thatcher, J. E., Blystone, A., Shelton, J. M., Galindo, C. L., Melegh, B., Srivastava, D., Olson, E. N. et al.** (2009). Thymosin beta4 mediated PKC activation is essential to initiate the embryonic coronary developmental program and epicardial progenitor cell activation in adult mice in vivo. *J. Mol. Cell. Cardiol.* **46**, 728-738.
**Carmona, R., Guadix, J. A., Cano, E., Ruiz-Villalba, A., Portillo-Sanchez, V., Perez-Pomares, J. M. and Munoz-Chapuli, R.** (2010). The embryonic epicardium: an essential element of cardiac development. *J. Cell. Mol. Med.* **14**, 2066-2072.
**Curado, S., Anderson, R. M., Jungblut, B., Mumm, J., Schroeter, E. and Stainier, D. Y.** (2007). Conditional targeted cell ablation in zebrafish: a new tool for regeneration studies. *Dev. Dyn.* **236**, 1025-1035.
**Gallagher, J. J., Sealy, W. C., Anderson, R. W., Kasell, J., Millar, R., Campbell, R. W., Harrison, L., Pritchett, E. L. and Wallace, A. G.** (1977). Cryosurgical ablation of accessory atrioventricular connections: a method for correction of the pre-excitation syndrome. *Circulation* **55**, 471-479.
**Gonzalez-Rosa, J. M., Padron-Barthe, L., Torres, M. and Mercader, N.** (2010). Lineage tracing of epicardial cells during development and regeneration. *Rev. Esp. Cardiol.* **63 Suppl. 2**, 36-48.
**Grimes, A. C., Stadt, H. A., Shepherd, I. T. and Kirby, M. L.** (2006). Solving an enigma: arterial pole development in the zebrafish heart. *Dev. Biol.* **290**, 265-276.
**Hsieh, P. C., Segers, V. F., Davis, M. E., MacGillivray, C., Gannon, J., Molkentin, J. D., Robbins, J. and Lee, R. T.** (2007). Evidence from a genetic fate-mapping study that stem cells refresh adult mammalian cardiomyocytes after injury. *Nat. Med.* **13**, 970-974.
**Ieda, M., Tsuchihashi, T., Ivey, K. N., Ross, R. S., Hong, T. T., Shaw, R. M. and Srivastava, D.** (2009). Cardiac fibroblasts regulate myocardial proliferation through beta1 integrin signaling. *Dev. Cell* **16**, 233-244.
**Itoh, G., Tamura, J., Suzuki, M., Suzuki, Y., Ikeda, H., Koike, M., Nomura, M., Jie, T. and Ito, K.** (1995). DNA fragmentation of human infarcted myocardial cells demonstrated by the nick end labeling method and DNA agarose gel electrophoresis. *Am. J. Pathol.* **146**, 1325-1331.
**Jennings, R. B., Murry, C. E., Steenbergen, C., Jr and Reimer, K. A.** (1990). Development of cell injury in sustained acute ischemia. *Circulation* **82 Suppl. 11**, 2-12.
**Jopling, C., Sleep, E., Raya, M., Marti, M., Raya, A. and Belmonte, J. C.** (2010). Zebrafish heart regeneration occurs by cardiomyocyte dedifferentiation and proliferation. *Nature* **464**, 606-609.
**Kajstura, J., Urbanek, K., Perl, S., Hosoda, T., Zheng, H., Ogorek, B., Ferreira-Martins, J., Goichberg, P., Rondon-Clavo, C., Sanada, F. et al.** (2010). Cardiomyogenesis in the adult human heart. *Circ. Res.* **107**, 305-315.
**Kikuchi, K., Holdway, J. E., Werdich, A. A., Anderson, R. M., Fang, Y., Egnaczyk, G. F., Evans, T., Macrae, C. A., Stainier, D. Y. and Poss, K. D.** (2010). Primary contribution to zebrafish heart regeneration by gata4(+) cardiomyocytes. *Nature* **464**, 601-605.
**Kim, J., Wu, Q., Zhang, Y., Wiens, K. M., Huang, Y., Rubin, N., Shimada, H., Handin, R. I., Chao, M. Y., Tuan, T. L. et al.** (2010). PDGF signaling is required for epicardial function and blood vessel formation in regenerating zebrafish hearts. *Proc. Natl. Acad. Sci. USA* **107**, 17206-17210.
**LaPage, M. J., Saul, J. P. and Reed, J. H.** (2010). Long-term outcomes for cryoablation of pediatric patients with atrioventricular nodal reentrant tachycardia. *Am. J. Cardiol.* **105**, 1118-1121.
**Lawson, N. D. and Weinstein, B. M.** (2002). In vivo imaging of embryonic vascular development using transgenic zebrafish. *Dev. Biol.* **248**, 307-318.
**Lepilina, A., Coon, A. N., Kikuchi, K., Holdway, J. E., Roberts, R. W., Burns, C. G. and Poss, K. D.** (2006). A dynamic epicardial injury response supports progenitor cell activity during zebrafish heart regeneration. *Cell* **127**, 607-619.
**Lie-Venema, H., van den Akker, N. M., Bax, N. A., Winter, E. M., Maas, S., Kekarainen, T., Hoeben, R. C., deRuiter, M. C., Poelmann, R. E. and Gittenberger-de Groot, A. C.** (2007). Origin, fate, and function of epicardium-derived cells (EPCDs) in normal and abnormal cardiac development. *ScientificWorldJournal* **7**, 1777-1798.
**Limana, F., Zacheo, A., Mocini, D., Mangoni, A., Borsellino, G., Diamantini, A., De Mori, R., Battistini, L., Vigna, E., Santini, M. et al.** (2007). Identification of myocardial and vascular precursor cells in human and mouse epicardium. *Circ. Res.* **101**, 1255-1265.
**Limana, F., Bertolami, C., Mangoni, A., Di Carlo, A., Avitabile, D., Mocini, D., Iannelli, P., De Mori, R., Marchetti, C., Pozzoli, O. et al.** (2009). Myocardial infarction induces embryonic reprogramming of epicardial c-kit(+) cells: Role of the pericardial fluid. *J. Mol. Cell. Cardiol.* **48**, 609-618.
**Limana, F., Capogrossi, M. C. and Germani, A.** (2010). The epicardium in cardiac repair: from the stem cell view. *Pharmacol. Ther.* **129**, 82-96.
**Mallo, M., Schrewe, H., Martin, J. F., Olson, E. N. and Ohnemus, S.** (2000). Assembling a functional tympanic membrane: signals from the external acoustic meatus coordinate development of the malleal manubrium. *Development* **127**, 4127-4136.
**Perner, B., Englert, C. and Bollig, F.** (2007). The Wilms tumor genes wt1a and wt1b control different steps during formation of the zebrafish pronephros. *Dev. Biol.* **309**, 87-96.
**Poss, K. D., Wilson, L. G. and Keating, M. T.** (2002). Heart regeneration in zebrafish. *Science* **298**, 2188-2190.
**Raya, A., Koth, C. M., Buscher, D., Kawakami, Y., Itoh, T., Raya, R. M., Sternik, G., Tsai, H. J., Rodriguez-Esteban, C. and Izpisua-Belmonte, J. C.** (2003). Activation of Notch signaling pathway precedes heart regeneration in zebrafish. *Proc. Natl. Acad. Sci. USA* **100 Suppl. 1**, 11889-11895.
**Saraste, A., Pulkki, K., Kallajoki, M., Henriksen, K., Parvinen, M. and Voipio-Pulkki, L. M.** (1997). Apoptosis in human acute myocardial infarction. *Circulation* **95**, 320-323.
**Serluca, F. C.** (2008). Development of the proepicardial organ in the zebrafish. *Dev. Biol.* **315**, 18-27.
**Smart, N., Dube, K. N. and Riley, P. R.** (2009). Coronary vessel development and insight towards neovascular therapy. *Int. J. Exp. Pathol.* **90**, 262-283.
**Sucov, H. M., Gu, Y., Thomas, S., Li, P. and Pashmforoush, M.** (2009). Epicardial control of myocardial proliferation and morphogenesis. *Pediatr. Cardiol.* **30**, 617-625.
**Tournoij, E., Weber, G. J., Akkerman, J. W., de Groot, P. G., Zon, L. I., Moll, F. L. and Schulte-Merker, S.** (2010). Mlck1a is expressed in zebrafish thrombocytes and is an essential component of thrombus formation. *J. Thromb. Haemost.* **8**, 588-595.
**Urbanek, K., Cabral-da-Silva, M. C., Ide-Iwata, N., Maestroni, S., Delucchi, F., Zheng, H., Ferreira-Martins, J., Ogorek, B., D'Amario, D., Bauer, M. et al.** (2010). Inhibition of Notch1-dependent cardiomyogenesis leads to a dilated myopathy in the neonatal heart. *Circ. Res.* **107**, 429-441.
**van den Bos, E. J., Mees, B. M., de Waard, M. C., de Crom, R. and Duncker, D. J.** (2005). A novel model of cryoinjury-induced myocardial infarction in the mouse: a comparison with coronary artery ligation. *Am. J. Physiol. Heart Circ. Physiol.* **289**, H1291-H1300.

**Vieira, J. M. and Riley, P. R.** (2010). Epicardium-derived cells: a new source of regenerative capacity. *Heart*. **97**, 15-19.
**Wagner, K. D., Wagner, N., Bondke, A., Nafz, B., Flemming, B., Theres, H. and Scholz, H.** (2002). The Wilms' tumor suppressor Wt1 is expressed in the coronary vasculature after myocardial infarction. *FASEB J.* **16**, 1117-1119.
**Watanabe, H., Eguchi, S., Miyamura, H., Hayashi, J., Aizawa, Y., Wakiya, Y. and Igarashi, T.** (1996). Histologic findings of long-term cryolesions in a patient with ventricular tachycardia. *Cardiovasc. Surg.* **4**, 409-411.
**Wills, A. A., Holdway, J. E., Major, R. J. and Poss, K. D.** (2008). Regulated addition of new myocardial and epicardial cells fosters homeostatic cardiac growth and maintenance in adult zebrafish. *Development* **135**, 183-192.
**Winter, E. M., Grauss, R. W., Hogers, B., van Tuyn, J., van der Geest, R., Lie-Venema, H., Steijn, R. V., Maas, S., DeRuiter, M. C., deVries, A. A. et al.** (2007). Preservation of left ventricular function and attenuation of remodeling after transplantation of human epicardium-derived cells into the infarcted mouse heart. *Circulation* **116**, 917-927.
**Yang, F., Liu, Y. H., Yang, X. P., Xu, J., Kapke, A. and Carretero, O. A.** (2002). Myocardial infarction and cardiac remodelling in mice. *Exp. Physiol.* **87**, 547-555.
**Zeisberg, E. M., Tarnavski, O., Zeisberg, M., Dorfman, A. L., McMullen, J. R., Gustafsson, E., Chandraker, A., Yuan, X., Pu, W. T., Roberts, A. B. et al.** (2007). Endothelial-to-mesenchymal transition contributes to cardiac fibrosis. *Nat. Med.* **13**, 952-961.